11th International Conference on Fast Sea Transportation
FAST 2011, Honolulu, Hawaii, USA, September 2011

Numerical Investigation of the Impact of SES-Waterjet Interactions and Flow Non-uniformity on Pump Performance

Yin Lu Young[1], Brant R. Savander[2] and Matthew R. Kramer[1]

[1]Dept. of Naval Architecture and Marine Engineering, University of Michigan, Ann Arbor, MI, USA
[2]Maritime Research Associates, L.L.C., Ann Arbor, MI, USA

ABSTRACT

The objective of this paper is to investigate the impact of SES-waterjet interactions and flow non-uniformity on pump performance via fully coupled computational fluid dynamics (CFD) simulations. The focus is on off-design conditions, such as near the hump speed. The CFD solver is first validated by comparing the numerical predictions with model-scale experimental measurements of a waterjet and an SES as separate components, followed by presentation of results for the full-scale response of an SES-waterjet system. The results show highly non-uniform flow at the inlet and throughout the waterjet. The predicted axial velocity contours inside the waterjet are in good general agreement with published experimental studies of hull-waterjet interactions. Work is currently underway to extend the modeling effort to consider the effect of shallow water and flexible seals on the coupled SES-waterjet response, and the resultant impact of flow non-uniformity on the hydroelastic response of the waterjet propulsion system.

KEY WORDS

Hull-propulsor interactions; SES; waterjet; flow non-uniformity; CFD; pump performance.

1.0 INTRODUCTION

Surface Effect Ship (SES) is a promising advanced ship technology that typically carries approximately 80% of its weight on an air cushion. The pressurized air is trapped by two rigid side hulls, as well as flexible bow and stern seals. By lifting most of the vessel above the water, the wetted area and hence frictional resistance are drastically reduced at high speeds.

To accommodate the shallow draft and slender side hulls of an SES, and to absorb the high thrust and power required for high-speed applications, waterjets are typically used as the primary propulsion system. In addition, waterjets are able to offer good manoeuvrability at all speeds via the use of a steerable nozzle to create vectored thrust.

A waterjet propulsion system typically has a flush mounted inlet and operates under complex three-dimensional (3-D) flow conditions. The 3-D flow is caused by ingestion of the hull boundary layer at the inlet, the adverse pressure gradient and flow separation inside the S-shaped duct, the blockage caused by the presence of the impeller shaft, the effect of shaft rotation, and the effect of impeller-stator interaction (Brandner & Walker 2007).

Waterjet propulsion for SESs is even more complicated because of inflow variation associated with interactions between the vessel, flexible seals, air cushion, and wave fields. The influence of flow non-uniformity may lead to early cavitation inception, which can cause thrust breakdown, blade vibration, and noise issues, particularly for heavily loaded applications. Inflow variations also have the potential to generate high-pressure pulses and large lateral loads on the duct and shaft. Moreover, the shallow draft and large air cushion of SES can cause air suction into the waterjet when operating in high seas, leading to a significant degradation in thrust and torque. The large load fluctuations can accelerate fatigue of the gears and prime movers, and may even affect vessel manoeuvrability.

Hence, the objective of this work is to investigate the impact of SES-waterjet interactions and flow non-uniformity on pump performance via fully coupled CFD simulations. The focus is on off-design conditions, such as near the hump speed. Future extensions of this work will consider the effects of littoral operations and hydroelastic response of the waterjet subject to spatial and temporal varying loads.

2.0 OVERVIEW OF ANALYSES

Given the computational and geometric complexity of an SES-waterjet system, and the lack of open experimental or numerical simulations on this topic, the waterjet and the SES are first considered separately through independent validation exercises. Results are then show for the predicted full-scale response of the coupled SES-waterjet system.

It should be noted that all the computations have been performed using the commercial CFD solver STAR-CCM+. Classical unsteady RANS (URANS) formulation details are not presented here, as they are readily available through references given in the STAR-CCM+ manuals. However, the models selected, domain setup, and other URANS-related topics are presented as they relate to the waterjet, SES, and coupled SES-waterjet computations.

3.0 VALIDATION: WATERJET ONLY

To validate CFD solver, numerical predictions are first compared with experimental measurements for the Office of Naval Research (ONR) AxWJ-1 waterjet geometry shown in Fig. 1. Model-scale tests results and references to the

geometric details can be found in Jessup et al. (2008). The model-scale AxWJ-1 has an interior casing diameter of 0.3048 m, a 7-blade rotor, and an 11-blade stator. The trailing edge of the nozzle has a diameter of 0.1615 m and the rotor tip gap is 7 mm.

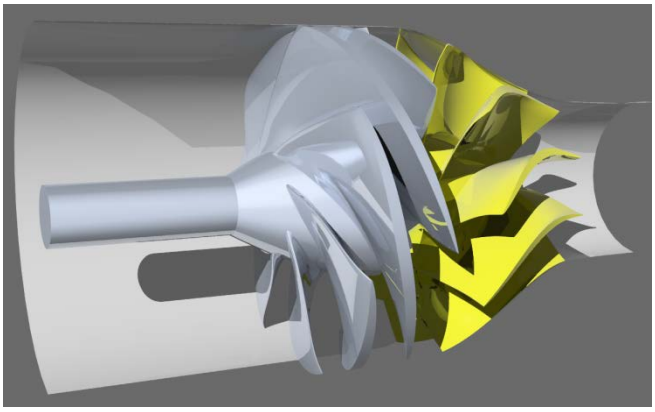

Fig. 1. Geometric model of waterjet AxWJ-1 used for URANS validation studies.

The AxWJ-1 design has undergone a series of tests at the closed-loop cavitation tunnel at John Hopkins University, which was especially designed to use index matching fluid and acrylic rotor blades to allow for enhanced flow visualization of tip gap cavitation (Wu et al. 2008). In addition to the index matching fluid, a subset of the test also utilized water as the fluid medium. A subset of the power performance data of AxWJ-1 can be found in Schroeder et al. (2009), where the experimental measurements were compared with multiphase URANS simulations.

The ultimate goal of this research is to investigate the transient hydroelastic response of heavily loaded waterjets subject to spatially and temporally varying inflow. Hence, an unstructured CFD mesh was used, and the entire rotor, stator, shaft, and casing are included in the polyhedron-based domain, as shown in Fig. 2.

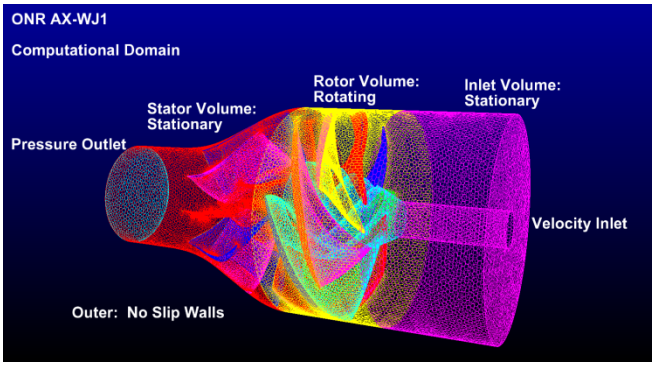

Fig. 2. Computational domain and polyhedron-based unstructured grid used for AxWJ-1 computations (flow is from right to left).

The computational domain is comprised of three volumes: inlet and stator volumes, which are stationary, and the rotor volume, which rotates relative to the other two volumes. Non-conformal mesh interfaces are used at shared boundary faces, where the flow solution is interpolated onto each shared volume face.

No-slip boundary conditions are applied at all solid surfaces, and the shaft rotation is applied as a boundary condition. A velocity inlet condition is used at the upstream boundary and a constant pressure outlet is defined at the nozzle outlet. Figure 3 shows the sample surface mesh density on the suction side of a rotor blade.

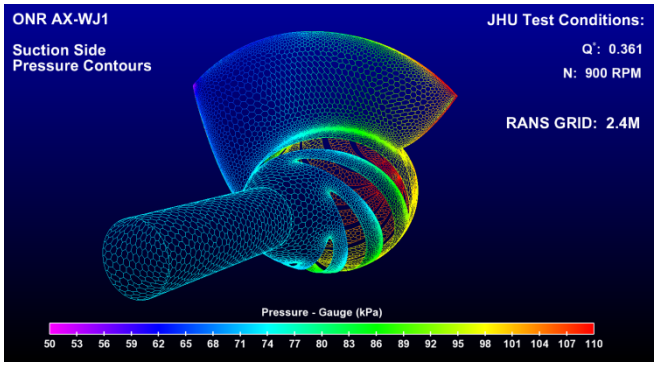

Fig. 3. Polyhedron-based surface mesh on one of the rotor blade assembly for waterjet AxWJ-1.

Boundary layer prisms are defined along the solid surfaces such that wall values of y^+ are within the following range:

$$10 < y^+ < 50 \tag{1}$$

with y^+ defined as,

$$y^+ = \frac{\rho u_\tau y}{\mu} \tag{2}$$

where u_τ is the friction velocity and y is the distance from the wall. The SST $k-\omega$ omega turbulence model (Wilcox 1998) was used for all simulations.

The flow coefficient is defined as:

$$Q^* = \frac{Q}{nD^3} \tag{3}$$

where Q is the volume flow rate, n is rotor rotation rate in units of rev/sec, and D is the rotor diameter. The design operating condition, Q^*=0.361, is selected for analysis, where the measured gauge pressure at the nozzle exit is 90.4 kPa for n=900 rpm.

To ensure spatial convergence, three different grids were examined during the AxWJ-1 computations: Grid-1 (fine), Grid-2 (medium), and Grid-3 (coarse). The total number of cell volumes was 3.9, 2.4, and 1.5 million for Grid-1, Grid-2, and Grid-3, respectively.

The predicted variations of the torque coefficient (K_Q as defined in Eq. 4) with the flow coefficient, Q^*, obtained using the 3 different grids are show in Fig. 4 together with the measured values from Wu et al. (2008).

$$K_Q = \frac{Q_\tau}{\rho n^2 D^5} \tag{4}$$

with Q_τ as the rotor torque.

As shown in Fig. 4, all three grids produced similar results, which suggest convergence. Error bars representing +/- 5% of the measured values are added for reference. In general, the URANS results compare well with the measured data from Wu et al. (2008). The predicted values are 3-5%

higher than the measured values in the lower Q^* range, and 4-6% higher in the higher Q^* range.

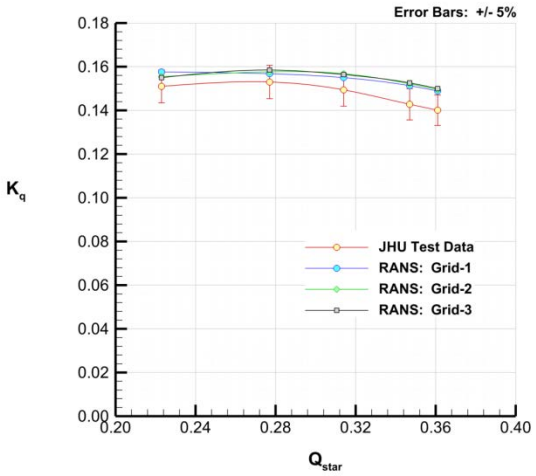

Fig. 4. Comparison of URANS results with test data from Wu et al. (2008) for the torque coefficient K_q as function of Q^* for AxWJ-1.

4.0 VALIDATION: SES ONLY

To validate the SES model, predictions are compared with bare hull resistance measurements for the model-scale ONR Transformable Craft (T-Craft), or DTMB model 5687, shown in Fig. 5. The tests, as described in Bishop et al. (2009), were conducted in the 98.3 m long x 6.1 m deep x 73 m wide manoeuvring and seakeeping (MASK) basin at the Naval Surface Warfare Center, Carderock Division (NSWCCD). The key dimensions of the T-Craft are provided in Table 1.

Fig. 5. DTMB model 5687 used for NSWCCD testing of ONR generic T-Craft.

Table 1. ONR T-Craft hull particulars**.**

Parameter	Symbol	Model-Scale	Full-Scale
Length overall	L_{OA}	2.53 m	76.35 m
Max. Beam	B	0.74 m	22.25 m
Cushion Length	L_C	2.22 m	67.14 m
Cushion Beam	B_C	0.55 m	16.50 m
Length-to-beam ratio	L/B	4.0	4.0
Displacement	Δ	55.1 kg	1588.6 t

The 100% cushion condition at a full-scale speed of 30 knots, which corresponds to a model scale speed of 5.5 knots, was selected for comparison with URANS predictions. The dynamic fluid body interaction (DFBI) computational domain is shown in Fig. 6. The trimmed hexahedral surface mesh on the hull is shown in Fig. 7. No-slip conditions are applied on all solid boundaries. Velocity inlet conditions are defined on the upstream, top, and bottom boundaries. Symmetry conditions are enforced on the side and centerline surfaces. The downstream boundary is prescribed as a pressure outlet. The entire computational grid moves with the hullform to avoid costly re-meshing. No waterjet is included in the model-scale SES simulations.

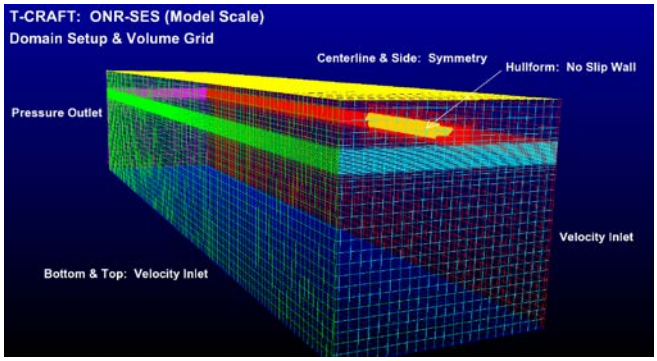

Fig. 6. URANS computational domain used for the T-Craft model scale resistance computations.

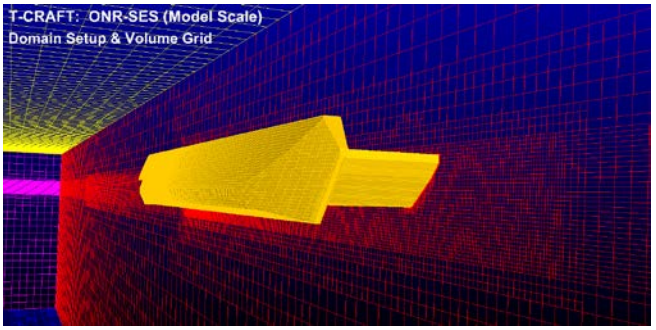

Fig. 7. URANS trimmed hexahedral surface mesh on the T-Craft hullform.

The Volume of Fluid (VOF) method in STAR-CCM+ is used to capture the free surface. Both the air and water phases are modeled as incompressible fluids. It should be noted that SES resistance modeling introduces two additional challenges compared to traditional mono-hull ships: the modeling of the air cushion, and the modeling of the flexible seals.

In this work, the pressure in the air cushion is created by a series of three momentum source volumes located at the forward, middle, and aft portions of the craft (see Fig. 11). The current URANS simulations assume the seals to be rigid surfaces, which represents a significant restriction in the approach. Since the equilibrium trim and draft are not known a priori, the height of the seals must be manually adjusted to avoid excessive seal immersion. Submerging the seals has the potential to corrupt the entire calculation by a) causing large and unrealistic seal drag, and b) distorting the wave pattern to a point that the results are of little value.

In the absence of a flexible seal model, the current analysis methodology is comprised of an iterative approach for

adjusting the fan momentum source strength coupled with geometric iteration of the seal position such that the cushion pressure, as measured in the experiments, is recovered without immersing the seals.

Figures 8 & 9 compare the observed and predicted wave patterns at a Froude number of *Fr*=0.6 (corresponding to a model scale velocity of 5.5 knots or full-scale velocity of 30 knots) in the 100% cushion configuration. A good qualitative comparison for the wave pattern was found between the model test and RANS solution. Good comparisons were also found between the predicted and measured resistance, as shown in Fig. 10.

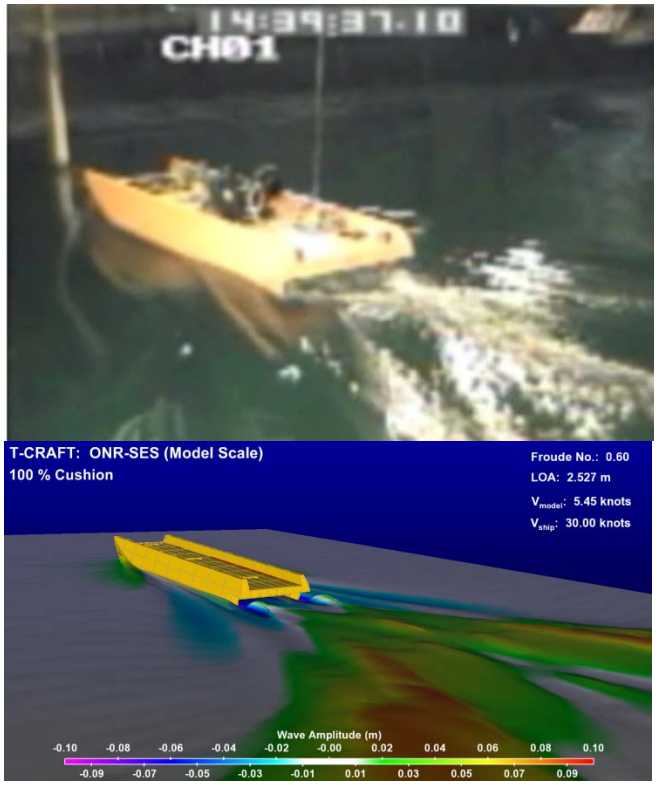

Fig. 8. Comparison of observed **(**Bishop et al., 2009) and predicted wave patterns for the model-scale T-Craft at *Fr*=0.6 and 100% cushion condition.

In the future, to avoid the overbearing seal position iterations, the research will focus on coupling a lower-order flexible seal model with the URANS computations. This seal development work is on-going and is expected to reach a publishable level within the next year.

5.0 ANALYSIS: FULL-SCALE SELF PROPELLED SES WITH TWO AxWJ-2 WATERJETS

The objective of this work is to establish a functional methodology to compute the spatially and temporally varying inflow to the pump inlet of a full-scale SES-waterjet system, and to evaluate the impact of flow non-uniformity on the pump performance. To properly simulate the pump inlet condition, the full waterjet system, which includes the SES, inlet, rotor, stator, and nozzle must be included in the model. Figure 11 shows a bottom view of the ONR T-Craft fitted with two AxWJ-2 waterjets. This figure also shows the three inlets used to pressurize the air cushion volume. Details of the AxWJ-2 waterjet design and model-scale performance data could be found in Michael et al. (2008) and Andersson (2010), respectively.

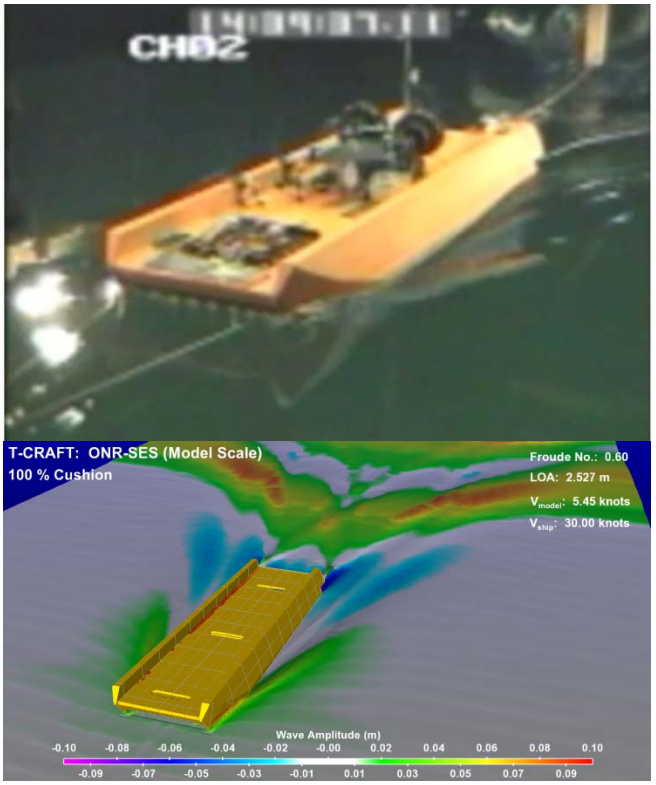

Fig. 9. Comparison of observed (Bishop et al., 2009) and predicted wave patterns for the model-scale T-Craft at Fr=0.6 and 100% cushion condition.

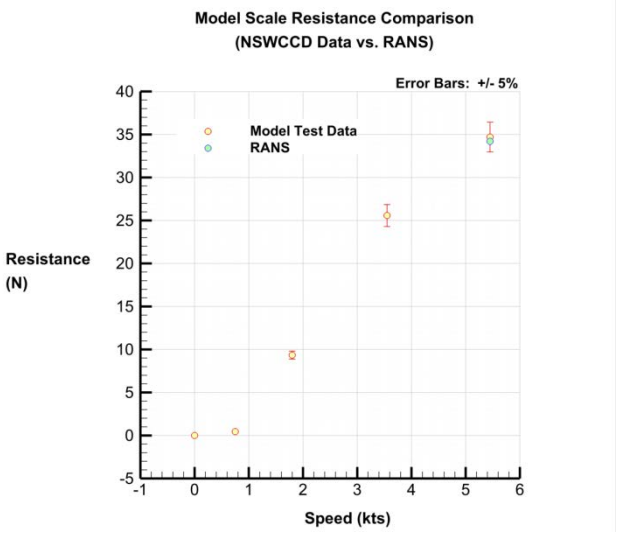

Fig. 10. Comparison of model scale resistance data with URANS predictions for ONR T-Craft model DTMB 5687.

Figure 12 shows two close-up views of AxWJ-2 fitted on the stern portion of the side hulls. To overcome the full-scale resistance, waterjet-hull matching required the size of the full-scale rotor diameter to be 1.7 m. The assumed inlet duct housing is representative of commercially available waterjet systems.

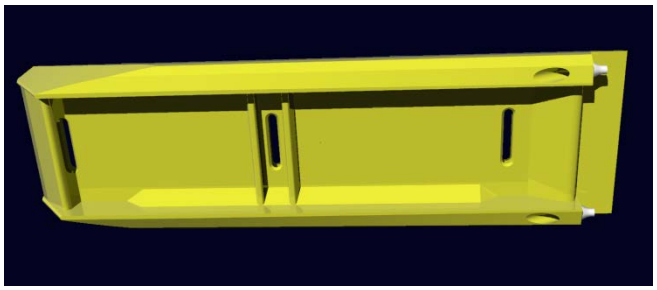

Fig. 11. Geometric model used for full scale computations of T-Craft being propelled by ONR waterjet AxWJ-2.

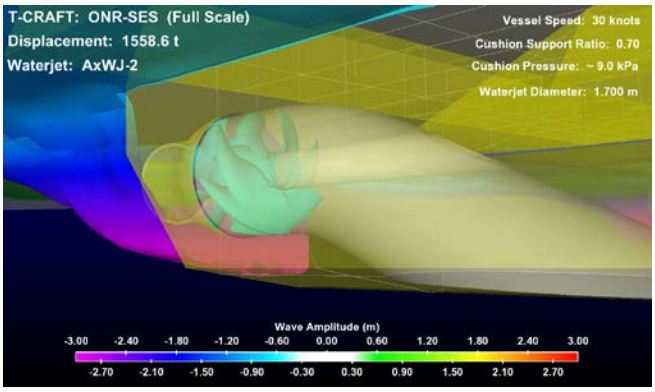

Fig. 12. Full-scale ONR waterjet AxWJ-2 used for self-propelled computation of generic ONR T-Craft.

Figure 13 shows a close-up view of the surface mesh for both the stator and rotor volumes. Topologically, the computational domain is a combination of the two meshing strategies discussed in the prior sections. The far-field tank domain utilizes a fixed trimmed hexahedral mesh. The trim and draft position of the SES was determined from steady resistance calculation at 30-knots with the waterjet inlets closed.

The stator and rotor domains are composed of unstructured polyhedron grids connected via non-conformal and in-place interfaces. Similarly, the tank domain communicates with the stator and rotor domains through non-conformal interfaces located at the nozzle exit, and the entrance to the inlet duct. Shaft rotation is considered by fixing the angular velocity at the shaft surface.

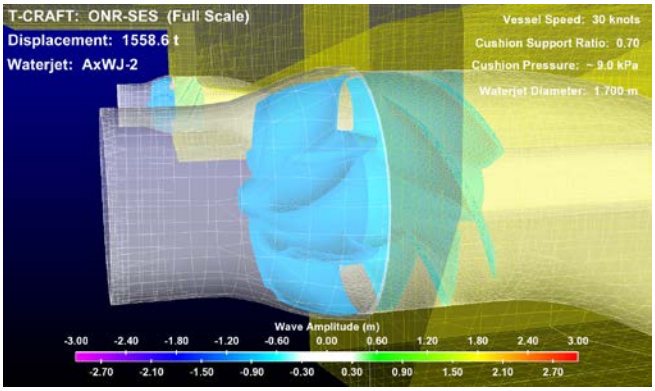

Fig. 13. View of stator and rotor surface mesh used for the full-scale self-propelled computation.

The number of computational cell volumes is approximately 3 million, which are divided equally among the three computational volumes: the tank, rotor, and stator.

Figure 14 shows the self-propelled T-Craft at a vessel speed of 30 knots and a waterjet rotational speed of n = 440 RPM. The lower image shows the T-Craft from the aft looking forward perspective, which reveals the presence of the waterjets.

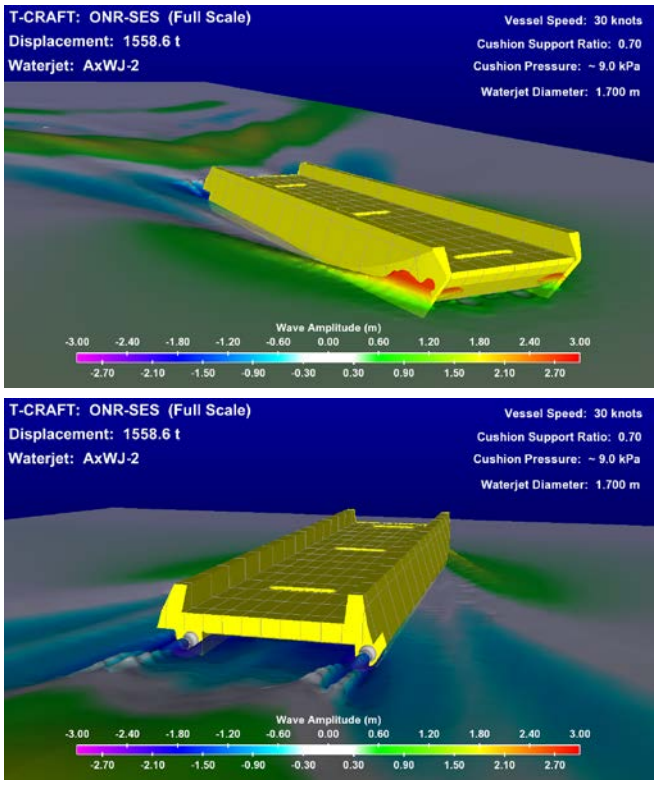

Fig. 14. Wave amplitude contours for T-Craft operating in the self-propelled case at 30 knots, and n = 440 RPM. Top: forward-looking-aft. Bottom: aft-looking-forward.

The computational sequence was to first allow the free surface to stabilize, which was achieved with a large time step size that corresponded to a rotor angular displacement of approximately 15 degrees. Once the free surface was established, the time step size was decreased such that the rotor angular displacement was in the range of 2-3 degrees. The final step in the computational process was to adjust rotor rotational speed such that waterjet thrust was equal to vessel resistance. For the 30 knot case, the equilibrium rotor speed was found to be n = 440 RPM.

Figure 15 shows streamlines in the waterjet inlet area, which may be used to define the inlet capture area. Note that no appreciable interaction is shown between the inlet streamlines and the air cushion free surface for this particular operating condition.

Figure 16 provides the gauge pressure contours on both the suction and pressure sides of the rotor, respectively, for the 30 knots, n = 440 RPM operating condition. In the current effort, cavitation has yet to be modeled. The results indicate that the blade pressures over a large area on the suction side, and near the leading edge at the root region on the pressure

side, are below the vapor pressure of -98 kPa gauge, i.e. cavitation is expected. It is important to note that the pressure contours are different on each blade due to flow non-uniformity.

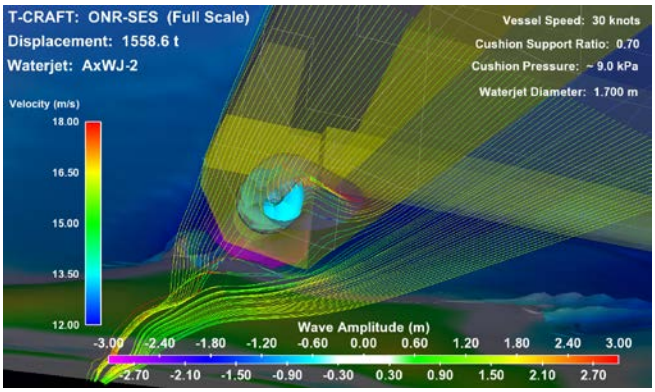

Fig. 15. Streamlines in way of waterjet inlet for the self-propelled T-Craft operating at a speed of 30 knots and a rotor speed of 440 RPM.

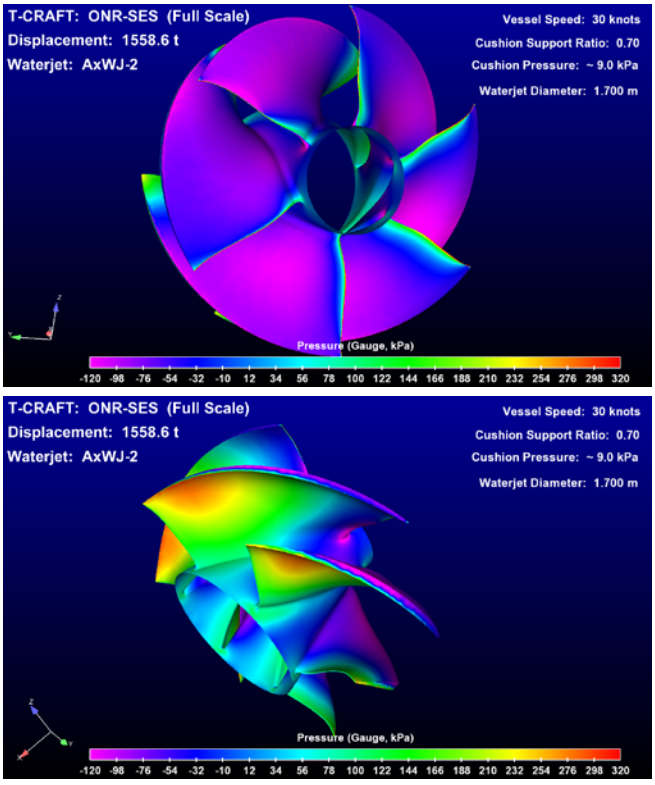

Fig. 16. Gauge pressure contours on the AxWJ-2 waterjet rotor with a rotor speed of n = 440 RPM and vessel speed of 30 knots. Top: suction side. Bottom: pressure side.

The pressure contours for the stator are provided in Fig. 17, which shows that cavitation is also expected over a significant portion of the suction side of the blades. In the conference presentation, the authors will show results of the current 30-knot case with the cavitation model activated.

The ITTC definitions for station locations in a waterjet system are shown in Fig. 18. The stations of interest for the current study are the waterjet inlet (station-1), rotor inlet (station-3), and nozzle exit (station-6).

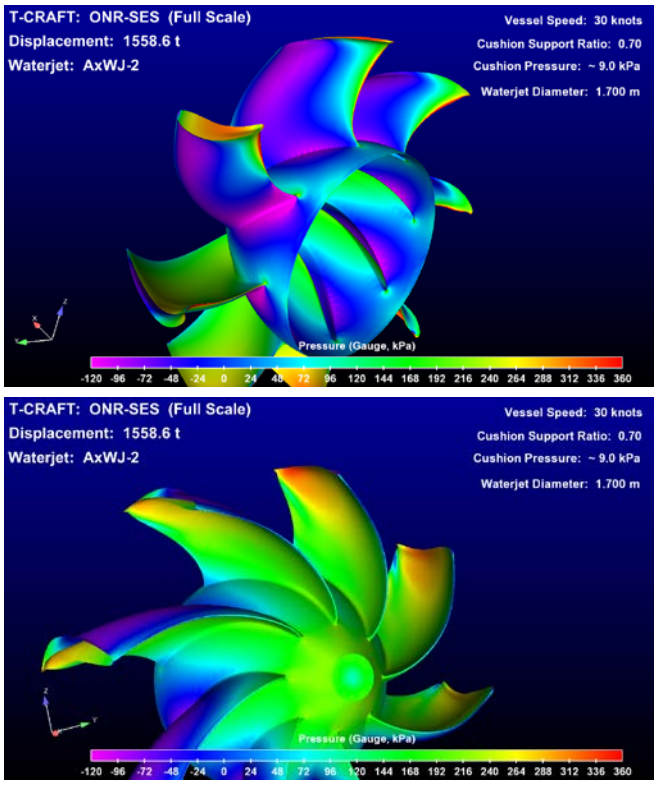

Fig. 17. Gauge pressure contours on the AxWJ-2 waterjet stator with a rotor speed of n = 440 RPM and vessel speed of 30 knots. Top: suction side. Bottom: pressure side.

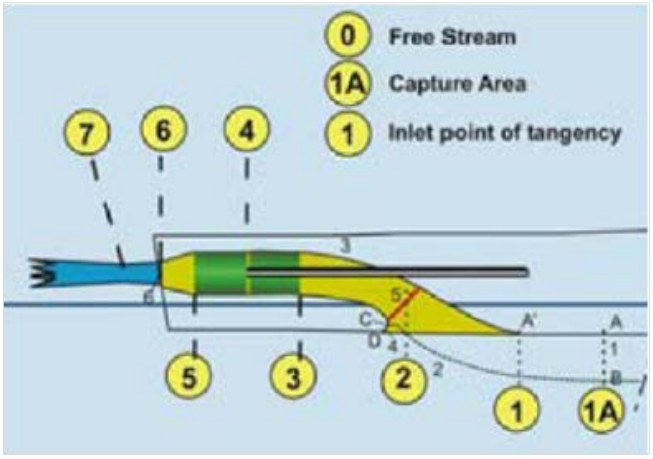

Fig. 18. ITTC convention for velocity station for waterjet systems (ITTC 2005).

The top image of Fig. 19 shows the axial velocity contours at ITTC station-1. This figure clearly shows the flow accelerating into the duct system with a maximum speed of approximately 36 knots. It also illustrates the 3-D nature of the inflow due to the ingested boundary layer and the inlet geometry.

The axial velocity contours for station-3 are shown in the middle figure of Fig. 19, which shows significant spatial variation of the axial velocity contour due to flow non-uniformity at station-1, the 3-D geometry of the pump housing, and interactions with the rotor and the rotating shaft.

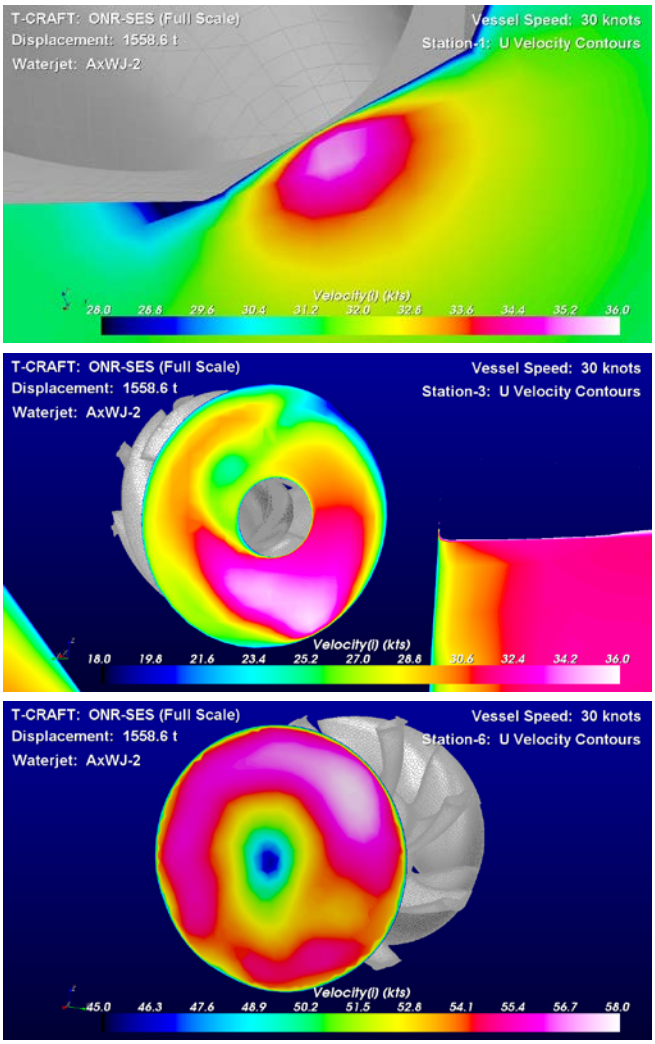

Fig. 19. Axial velocity contours for the case of vessel speed = 30 knots and the rotor speed n = 440 RPM. The jet velocity ratio (JVR) in this operating condition is 1.79. Top: station-1. Middle: station-3. Bottom: station-6.

Finally, the axial velocity contours for station-6 is provided in the bottom image of Fig. 19. The averaged velocity over the station-6 area reveals a jet velocity ratio (JVR) of 1.79. The JVR is defined as the circumferentially averaged value of the axial velocity at station-6 non-dimensionalized by the vessel speed, which is 30 knots.

The flow non-uniformity present in the station-3 velocity contours leads in time varying forces on individual components of the waterjet. The pattern of flow non-uniformity for station-1 and station-3 show qualitatively similar behavior to the experimental results of Jessup et al. (2008). However, the pattern for station-6 shows a much different behavior than those observed in the experimental study by Jessup et al. (2008), where the effect of the stator blades could be clearly distinguished. It should be noted that the predictions shown in Fig. 19 corresponds to full-scale simulations of an SES propelled by two AxWJ-2, while the experimental results shown in Jessup et al. (2008) corresponds to model-scale simulation of a high-speed monohull propelled by four AxWJ-1. Nevertheless, the primary discrepancy is suspected to be scaling effects because independent grid convergence study of the waterjet simulation has already been conducted (see Fig. 4), and the effect of the cushioned space seems to have negligible influence on the streamlines to the pump inlet.

Figure 20 provides the predicted time history of the total thrust acting on the pump, and the thrust acting on one of the rotor blades, for approximately three rotor revolutions. The results show that the fluctuation on the individual blade loads is approximately 30% of the mean values, while the fluctuations on the net shaft loading are negligible compared to the mean values.

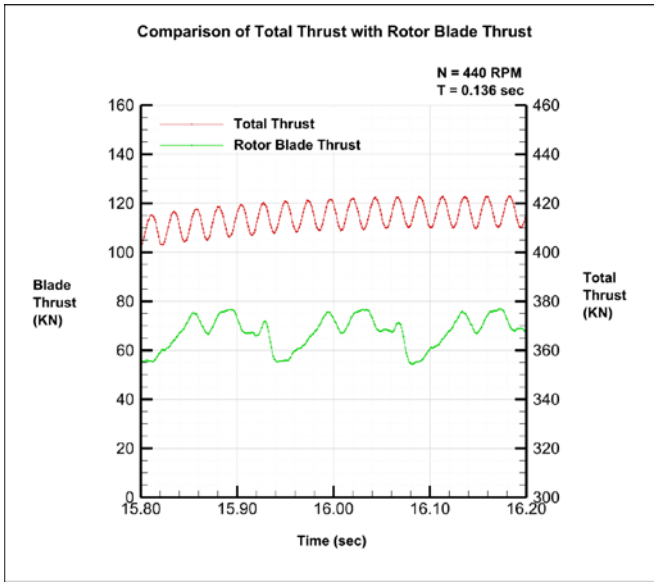

Fig. 20. Total waterjet thrust, which includes the rotor, stator, hub and casing for the case of the T-craft travelling at 30 knots and the rotor operating at a speed of 440 RPM. Individual blade thrust is also shown in this figure.

6.0 SUMMARY AND FUTURE WORK

Numerical validation studies with model-scale experimental data have been performed for a waterjet and an SES vessel individually with favorable results. Results are then shown for the full-scale response of a SES-waterjet system to demonstrate the effect of flow non-uniformity on the pump performance. It should be noted that typical waterjet designs and closed-loop cavitation tunnel studies of waterjets assume uniform inflow, which is not representative of realistic operating conditions. The effects of non-uniformity can lead to the early onset of cavitation, air ingestion, and unsteady blade and shaft loads, all of which can lead to excessive noise and vibrations issues.

The work presented in this paper demonstrates the simulation effort for a fully-coupled SES-waterjet system. The results clearly demonstrate the presence of flow non-uniformity at the inlet and through the various stations inside the waterjet, presence of unsteady cavitation, and load fluctuations on the rotor blades due to flow non-uniformity.

The analysis of the full-scale performance of the SES-waterjet system was limited to one operating condition.

Much more work is still anticipated to quantify the level of flow uniformity and resultant impact on pump performance across a range of flow conditions. Additional work will include experimental validation studies of the pump performance and thrust breakdown curves for ONR AxWJ-2 in spatially-uniform flow, as well as coupled simulation of the SES-waterjet system with consideration for cavitation in both deep and shallow water conditions. Finally, development of a reduced-order flexible seal model is currently underway to simulate the fluid-structure interaction response of the seals together with the SES-waterjet system, which is critical in the low Froude number regime. The ultimate goal of this work is to perform systematic studies to quantify the level of flow non-uniformity across a range of expected operating conditions, and its impact on hydrodynamic and hydroelastic pump performance.

ACKNOWLEDGEMENTS

The authors would like to thank ONR and Ms. Kelly Cooper for their generous support through ONR grant no. N00014-10-1-070. In addition, Matthew Kramer is supported under the National Defence Science and Engineering Graduate (NDSEG) fellowship.

We would also like to acknowledge the collaborative support of Prof. Katz' group from JHU and colleagues from NSWCCD Code 5800, who provided experimental data for the waterjet geometry and data, Mr. Steve Ouimette and Mr. Andy Silverman for providing the SES geometry and data, and Mr. Robert Wilson for his valuable input and advice.

REFERENCES

Andersson, L. (2010). "ONR AxWJ-2, Pump Loop Test." Rolls-Royce Hydrodynamic Research Centre Report PR-1223, Kristinehamm, Sweden.

Bishop, R.C., Silver, A.L., Tahmasian, D., Lee, S.S., Park, J.T, Snyder, L.A. & Kim, J. (2009). "T-Craft Seabase Seakeeping Model Test Data Report." Naval Surface Warfare Center Carderock Division, NSWCCD-50-TR-2009/055.

Brandner, P.A. & Walker, G.J. (2007). "An Experimental Investigation into to the Performance of a Flush Waterjet Inlet." Journal of Ship Research **51**(1), pp.1-21.

ITTC (2005). "Testing and Extrapolation Methods: High Speed Marine Vehicles, Waterjets, Waterjet System Performance, Recommended Procedures and Guidelines." 24th International Towing Tank Conference.

Jessup, S., Donnelly, M., Fry, D., Cusanelli, D. & Wilson, M. (2008). "Performance Analysis of a Four Waterjet Propulsion System for a Large Sealift Ship." 27th Symposium on Naval Hydrodynamics, Seoul, Korea.

Schroeder, S., Kim, S.E. & Jasak, H. (2009). "Toward Predicting Performance of an Axial Flow Waterjet Including the Effects of Cavitation and Thrust Breakdown." 1st International Symposium on Marine Propulsors, Trondheim, Norway.

Wilcox, D.C. (1996). Turbulence Modeling for CFD. 2nd ed. DCW Industries, Inc., La Canada, CA, USA.

Wu, H., Soranna, F., Michael, T., Katz, J., and Jessup, S. (2008). "Cavitation Visualizes the Flow Structure in the Tip Region of a Waterjet Pump Rotor Blade." 27th Symposium on Naval Hydrodynamics, Seoul, Korea.

